TISSUE ENGINEERING: Part C
Volume 24, Number 1, 2018

DOI: 10.1089/ten.tec.2017.0316

termis
Tissue Engineering
& Regenerative Medicine
International Society

METHODS ARTICLE

Label-Free, High-Throughput Purification of Satellite Cells Using Microfluidic Inertial Separation

Brian C. Syverud, PhD,[1] Eric Lin, PhD,[2] Sunitha Nagrath, PhD,[2] and Lisa M. Larkin, PhD[1,3]

Skeletal muscle satellite cells have tremendous therapeutic potential in cell therapy or skeletal muscle tissue engineering. Obtaining a sufficiently pure satellite cell population, however, presents a significant challenge. We hypothesized that size differences between satellite cells and fibroblasts, two primary cell types obtained from skeletal muscle dissociation, would allow for label-free, inertial separation in a microfluidic device, termed a ''Labyrinth,'' and that these purified satellite cells could be used to engineer skeletal muscle. Throughout tissue fabrication, Labyrinth-purified cells were compared with unsorted controls to assess the efficiency of this novel sorting process and to examine potential improvements in myogenic proliferation, differentiation, and tissue function. Immediately after dissociation and Labyrinth sorting, cells were immunostained to identify myogenic cells and fibroblast progenitors. Remaining cells were cultured for 14 days to form a confluent monolayer that was induced to delaminate and was captured as a 3D skeletal muscle construct. During monolayer development, myogenic proliferation (BrdU assay on Day 4), differentiation and myotube fusion index (α-actinin on Day 11), and myotube structural development (light microscopy on Day 14) were assessed. Isometric tetanic force production was measured in 3D constructs on Day 16. Immediately following sorting, unsorted cells exhibited a myogenic purity of $39.9\% \pm 3.99\%$, and this purity was enriched approximately two-fold to $75.5\% \pm 1.59\%$ by microfluidic separation. The BrdU assay on Day 4 similarly showed significantly enhanced myogenic proliferation: in unsorted controls $47.0\% \pm 2.77\%$ of proliferating cells were myogenic, in comparison to $61.7\% \pm 2.55\%$ following purification. Myogenic differentiation and fusion, assessed by fusion index quantification, showed improvement from $82.7\% \pm 3.74\%$ in control to $92.3\% \pm 2.04\%$ in the purified cell population. Myotube density in unsorted controls, 18.6 ± 3.26 myotubes/mm^2, was significantly enriched in the purified cell population to 33.9 ± 3.74 myotubes/mm^2. Constructs fabricated from Labyrinth-purified cells also produced significantly greater tetanic forces ($143.6 \pm 16.9\,\mu$N) than unsorted controls ($70.7 \pm 8.03\,\mu$N). These results demonstrate the promise of microfluidic sorting in purifying isolated satellite cells. This unique technology could assist researchers in translating the regenerative potential of satellite cells to cell therapies and engineered tissues.

Keywords: two-photon, optical imaging, skeletal muscle, microfluidics, tissue engineering

Introduction

Skeletal muscle has the ability to regenerate itself in response to damage,[1] largely due to the presence of potent muscle progenitor cells.[2] As the most abundant tissue in the body,[3] skeletal muscle requires this regenerative capacity for maintaining homeostasis and restoring function after injury. The resident skeletal muscle stem cell, the satellite cell, plays an essential role in repairing muscle damage.[4,5] In cases of severe injury, however, the native skeletal muscle repair mechanism is overwhelmed, and external intervention is indicated. A prime example is volumetric muscle loss (VML), defined as surgical or traumatic loss of a large volume of muscle tissue that leads to a functional deficit.[6] With VML, the ability of the damaged muscle to repair such a large defect through the native repair mechanism is insufficient, and fibrotic scar tissue instead accumulates in the defect site.[7] Current treatment options—free functional muscle transfer and composite tissue allotransplantation—involve grafting healthy muscle, innervation, and vasculature into the defect, but limitations such as donor-site morbidity and limited tissue availability often prevent complete recovery.[8–10] In addition,

Departments of [1]Biomedical Engineering, [2]Chemical Engineering, and [3]Molecular and Integrated Physiology, University of Michigan, Ann Arbor, Michigan.

muscular dystrophies are a family of inherited degenerative disorders characterized by systemic muscle weakness.[11–13] Duchenne muscular dystrophy is particularly distressing, due to its early onset and the lack of an effective treatment.[14–16] To address these clinical challenges, researchers have proposed using satellite cells in cell therapy[17–20] or tissue engineering approaches.[21–25] Although other cell types have been implicated as contributors to skeletal myogenesis,[26–28] recent research shows that satellite cells act as the primary source of regeneration of adult skeletal muscle.[4,29] Due to this tissue-specific regenerative ability, satellite cells have tremendous therapeutic potential.

Obtaining a suitable population of satellite cells, however, presents a continuing challenge. Satellite cells are relatively few in number, only accounting for 2–7% of the nuclei associated with a muscle fiber,[28,30] and current isolation methods have difficulty yielding both the population size and purity required.[31–33] Enzymatic dissociation yields a large quantity of cells with mixed myogenic and nonmyogenic populations, requiring a need for additional purification,[20,32,34] whereas single fiber explant culture isolates small satellite cell populations with purity of 95% or higher.[35–37]

The prevailing technique is to combine enzymatic isolation techniques with subsequent purification methods, but each has its associated drawbacks. Preplating, allowing rapidly adhering nonmyogenic cell attachment to a substrate to obtain a purified population of nonadherent myogenic cells,[20,38,39] provides a technically simple and scalable approach for purification. It is limited, however, by sensitivity of the preplate timing and potential for loss of myogenic cells. Alternatively, fluorescence-activated cell sorting (FACS) has successfully purified CD34+/CD45–/Sca1– myogenic cells from the heterogeneous isolated cell population.[26,40–42] Because of the heterogeneity of surface markers within the satellite cell pool,[43,44] however, retention of the full satellite cell population is difficult. Furthermore, FACS requires modification of the cells being analyzed through the addition of exogenous dyes or the electrical perturbations of the sorting process itself.[45] Magnetic-activated cell sorting (MACS) is another purification method, using magnetic microbeads conjugated to antibodies for specific markers of interest.[46] Direct comparison to other methods indicated less efficient purification with MACS in comparison to preplating,[47] and concerns about labeling with microbeads have been raised as well. Microfluidic characterization and sorting of fluorescently labeled skeletal muscle cells has been demonstrated as an alternative,[43,48] but is currently limited to small throughputs of hundreds of cells or less. By examining the existing techniques, it is clear that an efficient, label-free, high-throughput method for purifying satellite cells following isolation is required.

Inertial microfluidics has the potential to fill this pressing need. The inertial migration of particles in a microfluidic device was first observed by Segré and Silberberg in the 1960 s[49] and recently described by Di Carlo.[50] The efficacy of such devices has been demonstrated for separating particles in fluids, and a similar approach was tested in this study to examine separation of cells in suspension. Thus, the physics behind inertial separation described below refer to forces acting on cells rather than particles. To summarize these forces, cells in straight microfluidic channels experience stresses that act over the channel surface: (1) normal stress that yields drag forces parallel to the flow direction, (2) shear stress that yields lift forces perpendicular to the flow direction, and (3) a wall lift effect in opposition to the shear stress.[50–52] Drag forces accelerate cells in the flow direction along laminar streamlines. In contrast, the lift forces cause cell migration across streamlines. The wall lift force is directed away from the channel walls and decays with increasing distance from the walls. The shear lift force depends on the shear gradient generated by the fluid flow, resulting in forces directed away from the center of the channel. The combination of these lift forces focuses the cells to certain equilibrium positions according to the density of particles and the geometry of microfluidic channel. In a curved channel, centrifugal effects induce secondary flow (Dean flow) on the cross section of the channel. The generated double recirculation (Dean Vortices), along with the aforementioned lift forces, migrate cells transversely. Cell migration is correlated to the cell size and the curvature of the channel, resulting in a new profile of equilibrium positions which separates distinct size classes of cells.[50] In our case, a typical skeletal muscle cell isolate contains a mixture of satellite cells ranging from 8 to 13 μm[37,43] and myofibroblasts ranging from 10 to 22 μm,[53,54] in addition to smaller populations of hematopoietic, neural, and immune cells (ranging from 6 μm for smaller red blood cells up to 30 μm for larger monocytes and macrophages).

A microfluidic device, termed ''Labyrinth,'' was previously designed for and applied in the separation of circulating tumor cells (15–25 μm) from white blood cells (7–12 μm) using inertial microfluidic-based separation.[55] It is a high-throughput (1800–2500 μL/min), continuous, and biomarker-independent microfluidic separation technology. The design of the Labyrinth (Fig. 1), inspired by the Labyrinth in Greek mythology, incorporates 11 loops and 56 corners in a total channel length of 637 mm. The loops have small curvature ratios and provide enough channel length for complete focusing of cells, whereas sharp right-angle corners have high curvature ratios to further enhance focusing of smaller cells. Four separate outlets are designed to collect the focused individual streams of cells with differing sizes. Combining these features, the Labyrinth enables the separation of cells in different size classes with high efficiency.

In this study, we demonstrate the power of inertial microfluidic separation for purification of isolated satellite cells. We hypothesized that the size difference between satellite cells and fibroblasts, two primary cell types obtained from chemical dissociation of muscle, would allow for label-free, inertial separation in a microfluidic device and that purified satellite cells could be used to engineer our skeletal muscle units (SMUs). Throughout the engineered tissue fabrication process described extensively in the previous work,[24,56–58] Labyrinth-sorted cells were compared with unsorted controls to assess the efficiency of the microfluidic separation process and to examine potential improvements in myogenic proliferation, differentiation, and overall engineered tissue function as a result.

Materials and Methods

Animal care

All animal care procedures followed *The Guide for Care and Use of Laboratory Animals*,[59] according to a protocol approved by the University Committee for the Use and Care

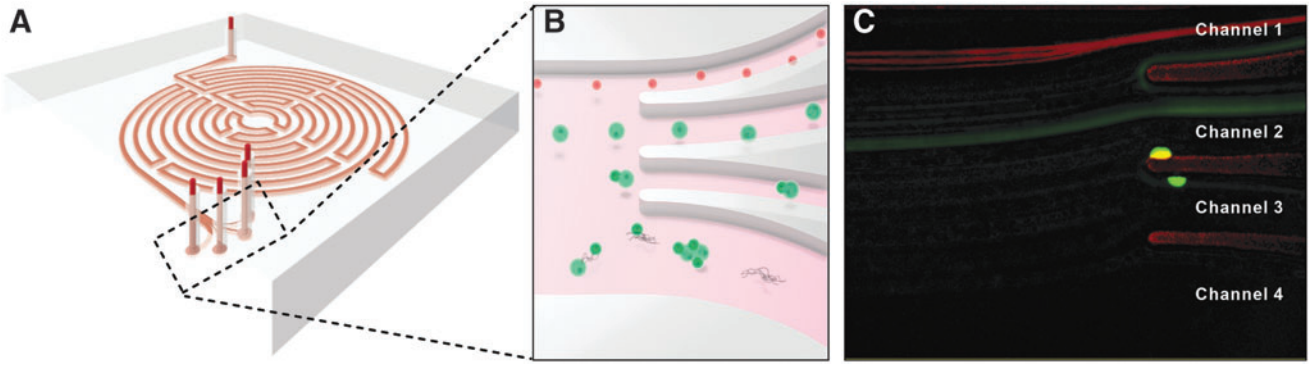

FIG. 1. Microfluidic Inertial Separation in the Labyrinth Device. A schematic representation of the Labyrinth is shown in **(A)**. Cells in suspension enter the device at the *top* of the image and rapidly flow (1800 μL/min) along the circuitous path created by a series of curved channels. Dean forces proportional to cell size and channel curvature act on the cells transversely to the flow direction, separating distinct size classes of particles at the outlets as pictured in **(B)**. Specifically, we intended to separate satellite cells, with a size range of 8–13 μm, from myofibroblasts, with a typical diameter of 10–22 μm. The Labyrinth was designed to focus the smaller satellite cells into Channel 1 (*top*), larger myofibroblasts into Channel 2 (second from *top*), and cell aggregates and debris into Channels 3 and 4 (*bottom*). **(C)** Visualization of a mixed population of Pax7+ satellite cells expressing *red* tdTomato fluorescence and Achilles tendon fibroblasts labeled with CellTracker *Green* fluorescent dye during sorting confirmed efficient separation of these two cell types based on their difference in size.

of Animals. Validation of the Labyrinth was performed using fluorescently labeled primary mouse cells. Pax7-positive satellite cells expressing red fluorescence were isolated from a transgenic Pax7CreERT2-r26-tdT mouse, provided by collaborators in the laboratory of Dr. Chris Mendias, Department of Orthopedic Surgery at the University of Michigan. To induce tdTomato fluorescence expression, mice were injected intraperitoneally with tamoxifen (Sigma-Aldrich, St. Louis, MO, cat. no. T5648) in corn oil (Sigma, cat. no. C8267) at a dose of 0.5 mg diluted to 10 mg/mL. Injections were repeated for 5 consecutive days, and cells were isolated at least 10 days after the final injection. Mouse Achilles tendon fibroblasts were isolated from C57BL6 mice supplied by Charles River Laboratories, Inc. (Wilmington, MA) and were fluorescently labeled using CellTracker Green CMFDA Dye (Life Technologies, Carlsbad, CA, cat. no. C7025) according to the manufacturer's protocol. A total of $n = 6$ mice were used in this study, $n = 3$ for initial optimization of the device flow rate, and $n = 3$ for characterization of the sorted cell purity.

SMUs were engineered using soleus muscles and bone marrow from 145 to 155 g female Fischer 344 rats, supplied by Charles River Laboratories. Animals acclimated to colony conditions for 1 week before any procedure and were fed Purina Rodent Chow 5001 and water *ad libitum*. Intraperitoneal injections of sodium pentobarbital (50 mg/kg for mice, 65 mg/kg for rats; Merck Animal Health, Madison, NJ, NADA # 119–807) were used to induce a deep plane of anesthesia. Supplemental pentobarbital doses were administered as required to maintain adequate anesthesia depth. In this study, a total of $n = 6$ rats were used to generate the data presented.

Muscle dissection and cell isolation

From rats, both soleus muscles were removed under aseptic conditions and sterilized in 70% ethanol. All hindlimb muscles were dissected when isolating mouse muscle cells. The muscles were then minced using a razor blade, placed under ultraviolet light for 15 min in 15 mL of Ham's F12 (Gibco BRL, Carlsbad, CA, cat. no. 11765–047), and added to a dissociation solution consisting of 32 U dispase (1.8 U/mg; Gibco, cat. no. 17105–04) and 2390 U type IV collagenase (239 U/mg; Gibco, cat. no. 17104–019) in 20 mL of Ham's F12. The mixture was maintained at 37°C with agitation for 90 min. The resulting suspension was then filtered with a 100 μm mesh filter (Fisher Scientific, Waltham, MA, cat. no. 22363549) before centrifugation. The dissociation solution was aspirated off and the cells were resuspended in growth medium.

Microfluidic device fabrication

The mold for the polydimethylsiloxane (PDMS) device was fabricated following a standard protocol of soft lithography. Using a spin coater, a negative photoresist layer of SU-8 100 (MicroChem, Westborough, MA, cat. no. SU-8 100) was deposited onto silicon wafer with 2450 rpm rotation for 1 min. The wafer was then soft baked for 10 min at 65°C and 70 min at 95°C. A mask with the device geometry was aligned to the wafer and exposed to UV light for 20 s to cure the photoresist. Postexposure baking was applied for 3 min at 65°C and 10 min at 95°C. Next, the wafer was soaked in developer solution (MicroChem, cat. no SU-8 Developer) for 6 min and in isopropyl alcohol (Sigma, cat. no. W292907) for 1 min to remove the inactivated photoresist. It was finally hard baked for 4 min at 150°C–180°C. The resulting height of the mold on silicon wafer was 100 μm, and the width of the channel was 500 μm.

The flow chamber for Labyrinth was made from PDMS (Sylgard 184; Dow Chemical Corp., Midland, MI, cat. no. 4019862). Thirty microliters of Sylgard polymer base and 3 mL curing agent were thoroughly mixed and poured onto a silicon mold. The mixture was placed into a desiccator for 2 h to remove air bubbles from the mixture and then heated at 65°C overnight to harden the polymer. The polymer was

next cut into the desired shape, and punched with a needle for tubing insertion. The PDMS device was then bonded to standard size glass slides through plasma surface activation of oxygen. The bonded device was plumbed with 0.76-mm diameter tubes (Cole-Parmer, Vernon Hills, IL, cat. no. 06419-00).

Microfluidic inertial separation

The Labyrinth device was primed with 1% pluronic acid solution (Sigma, cat. no. P2443) in Dulbecco's Phosphate-Buffered Saline (DPBS; Fisher, cat. no. 14190144) at 100 μL/min for 10 min and then incubated for 10 min to prevent cell clotting on channel walls. Cell samples in suspension were then pushed through the Labyrinth at a flow rate of 1800 μL/min using a syringe pump (Harvard Apparatus, Holliston, MA, cat. no. 55-2222). After 60 s of flow stabilization, the products from each of the four Labyrinth outlets were collected separately.

Preparation of tissue-engineered bone and tendon anchors

As described in previous studies, bone and tendon constructs were fabricated to act as anchors onto which developing muscle monolayers could attach and fuse.[58,60] Bone marrow from both femurs of Fischer 344 rats was removed under aseptic conditions. Isolated bone marrow cells were plated in 100-mm tissue culture plates (BD Falcon, Franklin Lakes, NJ). Following four passages to drive cells to the bone or tendon lineage, the confluent monolayers delaminated from the tissue culture plate and were pinned in cylindrical forms into PDMS-coated dishes. The resulting tissue constructs were maintained in 3D form for 2 days before being cut into 5-mm sections to be used as engineered bone–tendon anchors for construct implantation.

SMU formation

SMUs were engineered in 60-mm polystyrene plates (Fisher, cat no. 353002), and immunocytochemistry (ICC) was performed on 35-mm plates (Fisher, cat. no. 353001) as described previously.[58,60] Briefly, a substrate of PDMS was cured onto each plate, followed by coating with laminin (Natural Mouse Laminin, Gibco, cat. no. 23017-015) at 1 mg/cm^2. Isolated muscle satellite cells were seeded in muscle growth medium (MGM) at 600,000 cells per 60-mm plate or 150,000 cells per 35-mm plate. MGM contained 30 mL F-12 Kaighn's Modification Nutrient Mixture (Gibco, cat. no. 21127-022), 12.5 mL Dulbecco's modified Eagle's medium (DMEM; Gibco, cat. no. 11995-065), 7.5 mL fetal bovine serum (FBS; Gibco, cat. no. 10437-028), 2.4 ng/mL basic fibroblast growth factor (bFGF; PeproTech, Rocky Hill, NJ, cat. no. 100-18B), and 0.5 mL antibiotic–antimycotic (ABAM; Gibco, cat. no. 15240-062). After initial plating for 4 days to allow attachment, cells were subsequently fed MGM every 2 days until becoming fully confluent on Day 7 with a network of elongating myotubes. At this point, 5 mm tissue-engineered bone–tendon anchors were pinned onto the cell monolayers at a spacing of 2.5 cm, and the medium was switched to muscle differentiation medium (MDM). MDM was composed of 35 mL M199 (Gibco, cat. no. 11150-059), 11.5 mL DMEM, 3 mL FBS, 500 μL ABAM, 500 μL 1 μM dexamethasone (Sigma, cat. no. D4902), 50 μL insulin–transferrin–selenium-X (Sigma, cat. no. I1884), and 36.2 μL 50 mM ascorbic acid 2-phosphate (Sigma, cat. no. A8960). After a week on MDM, resupplied every other day, the monolayers delaminated from the plates on Day 14, rolling into cylindrical muscle constructs, held at length by the engineered bone anchors.

Immunocytochemical analysis

At specific time points during SMU fabrication, samples were fixed in 20°C methanol for 10 min and set aside for ICC. Samples were washed for 10 min in 0.1% Triton X-100 (Sigma, cat. no. T8787) in DPBS (PBST) and blocked with PBST containing 3% Bovine Serum Albumin (PBST-S; Sigma, cat. no. A2153) at room temperature. Samples were then incubated overnight at 4°C with primary antibodies diluted in PBST-S. Immunofluorescent staining was performed using the following primary antibodies: mouse monoclonal anti-desmin (1:20 dilution; Developmental Studies Hybridoma Bank, Iowa City, IA, cat. no. D3), mouse monoclonal anti-Pax7 (1:100 dilution; Abcam, Cambridge, MA, cat. no. ab199010), rabbit polyclonal anti-PDGFRα (1:100 dilution; Santa Cruz Biotech, Dallas, TX, cat. no. sc-431), biotin-conjugated sheep polyclonal anti-BrdU (1:50 dilution; Abcam, cat. no. ab2284), mouse monoclonal anti-MyoD (1:100 dilution; BD Biosciences, San Jose, CA, cat. no. 554130), rabbit polyclonal anti-fibroblast-specific protein 1 (FSP1; 1:100 dilution; Abcam cat. no. ab27957), and mouse monoclonal anti-α-actinin (1:200 dilution; Sigma, cat. no. A7752).

Plates stained with anti-BrdU had previously been incubated for 24 h with a BrdU labeling reagent (Life Technologies, cat. no. 00-0103) in the MGM. Following three PBST washes for 5 min each, samples were incubated in 1:500 dilutions of Alexa Fluor anti-mouse, anti-rabbit, or streptavidin secondary antibodies (Life Technologies) for 3 h at room temperature. Following three washes in PBST for 15 min each, samples were preserved in ProLong Gold with DAPI (Life Technologies, cat. no. P36935) and cover slipped. Samples were examined and photographed with a Leica Inverted microscope, and images were analyzed using the ImageJ software package (National Institutes of Health, Bethesda, MD). For ICC analysis, samples from each experimental group were fixed and stained (on Day 0 for Cytospin; Day 4 for BrdU; and Day 11 for α-actinin). Cells fixed on Day 0 were attached to microscope slides through Cytospin at 800 RPM for 8 min. From each sample, ten random areas were imaged, and the number of positively stained nuclei in each image was counted.

Myotube fusion index calculation

From the α-actinin images, the percentage of myogenic nuclei was first calculated by dividing the total number of DAPI-positive nuclei by the number of nuclei associated with an α-actinin-positive cell. The structural protein α-actinin is often used to identify Z-lines in skeletal muscle sarcomeres, but α-actinin is also expressed in the stress fibers of myoblasts before fusion.[61–63] To calculate myotube fusion index, α-actinin-positive muscle cells were quantified depending on the number of nuclei contained. Specifically, muscle cells were divided into groups with one, two, three,

and four or more nuclei, and these values were reported as a percentage of the total number of α-actinin-positive nuclei.

Myotube size and density analysis

On Day 14 after initial seeding, light micrographs of developing monolayers were captured. Specifically, ten random areas from each 60-mm plate were imaged. Every myotube from these images was then measured in ImageJ to determine its size and the overall density of the myotube network.

SMU contractile measurements

SMU force production was measured on Day 16 following roll-up into 3D cylindrical form. The protocol for measuring contractility of engineered muscle constructs has been described previously.[24,64,65] Briefly, the pin on one end of the SMU was attached to a force transducer with a 0–5 mN range and a 0.4 μN resolution (World Precision Instruments, Sarasota, FL, cat. no. SI-KG7A). Platinum wire electrodes were placed along either side of the SMU for field stimulation. The temperature of the construct was maintained at 37° C, using a heated aluminum platform. Twitch contractions were elicited using a single 2.5 ms pulse at 10, 30, 60, and 90 mA, whereas tetanic force was determined using a 1 s train of 2.5 ms pulses at 90 mA and 10, 20, 40, 60, and 80 Hz. Data files for each peak twitch force and peak tetanic force trace were recorded and subsequently analyzed using LabVIEW 2013 (National Instruments, Austin, TX).

Statistical analysis

Based on previous data in which force generation was the main parameter of interest, a sample size of 8 plates or SMUs per experimental group is required to test for statistically significant differences ($\alpha = 0.05$) at power levels of at least 0.9. Thus, samples sizes of at least $n = 8$ plates or SMUs were used in each group to ensure the power to detect differences. Values are presented as mean ± standard error. Measurements of significant differences between means were performed using GraphPad Prism 7 (GraphPad Software, Inc., La Jolla, CA). Mean was compared using either a Student's *t*-test or one-way ANOVA with Tukey's *post hoc* comparisons. Differences were considered significant at $p < 0.05$.

Results

Initial validation of microfluidic satellite cell purification

The sorting efficiency of the Labyrinth microfluidic device was validated using fluorescently labeled primary mouse cells. A combination of Pax7-positive satellite cells ubiquitously expressing red tdTomato fluorescence and Achilles tendon fibroblasts labeled with CellTracker Green fluorescent dye were separated at several different fluid flow rates. Visualization of the fluorescent cells during sorting (Fig. 1C) indicated improved separation distances between satellite cells and fibroblasts at lower flow rates (1800 μL/min: 148 μm, 2000 μL/min: 135 μm, 2200 μL/min: 128 μm, 2500 μL/min: 112 μm). Based on these results, a flow rate of 1800 μL/min was used for all subsequent sorting runs. Sorting of the fluorescently labeled cell populations was repeated, and the separated cells were quantified with a hemocytometer (Table 1). From these results, it is clear the Labyrinth separated the cell populations as intended, significantly enriching the satellite cell population from 33.3% ± 3.36% in unsorted controls to 66.5% ± 6.03% in Channel 1 ($p = 0.015$) and the fibroblast population from 43.2% ± 2.57% unsorted to 70.6% ± 1.28% in Channel 2 ($p > 0.001$).

Isolated cell populations immediately following microfluidic sorting

The Labyrinth device demonstrated similar sorting efficiency in separating isolated primary rat cells (Table 1). Following isolation and sorting, cells attached to microscope slides through Cytospin were immunostained with Pax7 and desmin to characterize myogenic cells and PDGFRα to identify fibroblast progenitors. Analysis of images from the separated cell populations indicated that a purified population of myogenic cells was evident in Channel 1 of the Labyrinth device. Specifically, compared with the unsorted muscle dissociation, with a myogenic cell purity of 39.9% ± 4.0%, Labyrinth-sorted cells were significantly enriched with myogenic cells, approximately two-fold, to 75.5% ± 1.6% ($p < 0.001$). Because of their larger cell size, the fibroblast cells were separated into Channels 2, 3, and 4 by the Labyrinth device. In comparison to the unsorted dissociation with a fibrogenic cell purity of 45.6% ± 3.1%, channels 2, 3, and 4

Table 1. Purity of Separated Cell Populations Following Sorting

	Unsorted control	*Sorted channel 1*	*Sorted channel 2*	*Sorted channel 3*	*Sorted channel 4*
(A) Primary mouse cells					
Pax7+ Purity ($n = 3$ mice)	33.3% ± 3.36%	66.5% ± 6.03%[a]	27.2% ± 5.76%	21.2% ± 11.6%	0.00% ± 0.00%
Fibroblast purity ($n = 3$ mice)	43.2% ± 2.57%	11.9% ± 4.81%	70.6% ± 1.28%[a]	17.4% ± 2.96%	0.18% ± 0.13%
(B) Primary rat cells					
Myogenic purity ($n = 6$ rats)	39.9% ± 3.99%	75.5% ± 1.59%[a]	27.5% ± 4.17%	12.0% ± 1.56%	7.36% ± 1.30%
Fibrogenic purity ($n = 6$ rats)	45.6% ± 3.14%	21.9% ± 1.94%	57.4% ± 2.65%	60.8% ± 4.86%[a]	78.3% ± 4.47%[a]

Purity in mouse cells ($n = 3$ animals) **(A)** refers to the percentage of fluorescent cells (red for Pax7+ satellite cells, green for fibroblasts) among the total cells counted in each Labyrinth channel. It is worth noting that very few cells were present in Channel 4, and none of these cells was Pax7+. In rat isolates ($n = 6$ animals) **(B)**, cells were characterized as myogenic if expressing either Pax7 or desmin, and fibrogenic based on expression of PDGFRα. The difference in sorted mouse and rat populations, evident in Channels 3 and 4, can be explained by the methods used to label these cells. The mouse cells contained a population of unlabeled fibroblasts from enzymatic digestion of the muscle biopsy. It is expected that these unlabeled fibroblasts represented a sizeable portion of the mouse cells sorted into Channels 3 and 4. In all tables and figures, values are presented as mean ± standard error.

[a]indicates significant increases relative to unsorted controls.

demonstrated increased fibroblast purities of 57.4% ± 2.7% ($p = 0.1091$), 60.8% ± 4.9% ($p = 0.023$), and 78.3% ± 4.5% ($p < 0.001$), respectively.

Effects of microfluidic sorting on cell proliferation

To assess the influence of the microfluidic separation process on cell proliferation, Labyrinth-sorted cells were seeded and cultured normally. ICC analysis was performed on Day 4 following seeding to identify proliferating cells expressing BrdU, a synthetic nucleoside analog of thymidine. Expression of MyoD and FSP1 was examined simultaneously to identify myogenic cells and matrix-secreting fibroblasts, respectively. From BrdU analysis of plates ($n = 10$), it was clear that microfluidic sorting did not have an effect on overall cell proliferation (Fig. 2). In unsorted controls 91.2% ± 1.2% of cells were proliferating, whereas cells sorted into Channel 1 of the labyrinth exhibited 91.6% ± 1.0% ($p = 0.556$). Costaining for MyoD, however, demonstrated a significant increase ($p = 0.004$) in proliferating myogenic cells sorted into Channel 1 (57.1% ± 3.0%) as compared with unsorted controls (44.3% ± 2.8%). In contrast, FSP1 costaining indicated that the percentage of proliferating fibrogenic cells in unsorted controls, 46.9% ± 1.9%, was significantly decreased to 34.5% ± 1.9% by microfluidic sorting ($p < 0.001$). It is worth noting that insufficient myogenic cells for seeding and SMU fabrication were present in Channels 2, 3, and 4, so only unsorted controls and Channel 1 cells were compared for this and subsequent analysis.

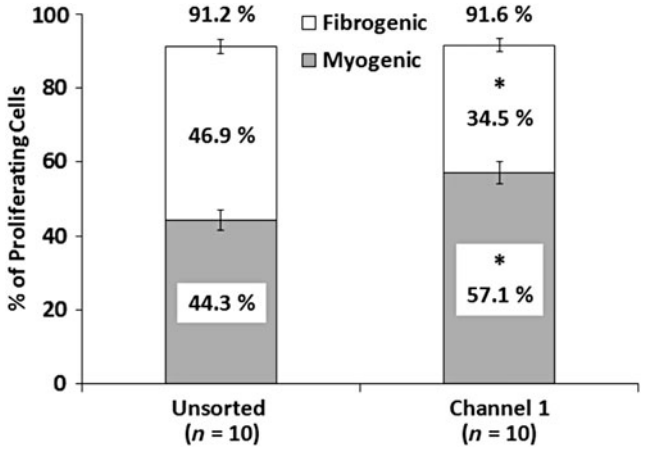

FIG. 2. Myogenic and Fibrogenic Proliferation of Sorted Cells. Incorporation of BrdU on Day 4 of SMU fabrication was used to identify proliferating cells. No difference in overall proliferation was observed between unsorted controls (91.2% ± 1.2%) and cells sorted into Channel 1 (91.6% ± 1.0%, $p = 0.556$), suggesting the sorting process did not adversely affect cell growth. Immunostaining for MyoD and FSP1 indicated myogenic and fibrogenic cells, respectively. Proliferating myogenic cells were significantly enriched ($p = 0.004$) after sorting into Channel 1 (57.1% ± 3.0%) as compared with unsorted controls (44.3% ± 2.8%). In contrast, FSP1 staining indicated by proliferating fibrogenic cells in unsorted controls, 46.9% ± 1.9%, were significantly decreased to 34.5% ± 1.9% by microfluidic sorting ($p < 0.001$). * Indicates statistical difference from control.

Myogenic differentiation and myotube fusion following microfluidic sorting

Myotube fusion index was measured to assess the ability of sorted cells to form a network of myotubes following microfluidic separation. Expression of α-actinin on Day 11 of SMU fabrication was used to identify fused myotubes and sarcomeric structure. Myotubes in both control and Channel 1 plates exhibited dense networks of longitudinally aligned myofibrils with advanced sarcomeric structure (Fig. 3A, B). Quantification of the number of nuclei associated with α-actinin-positive cells yielded a myotube fusion index value. From a *t*-test, the overall percentage of nuclei associated with cells expressing α-actinin in unsorted control plates ($n = 8$) of 52.0% ± 2.8% was not significantly different ($p = 0.142$) from plates seeded with cells sorted into Channel 1 57.0% ± 2.1% (Fig. 3C). However, the number of fused myotubes with four or more nuclei in unsorted control plates, 82.7% ± 3.7%, was significantly increased to 92.3% ± 2.0% in Channel 1 plates ($p < 0.001$, Fig. 3D).

Further analysis of the myotube network was performed on Day 14 of the fabrication protocol using light microscopy. The average myotube diameter in unsorted controls ($n = 10$) was 16.0 ± 1.3 μm. This value was nearly identical ($p = 0.938$) to the myotube diameter of 16.18 ± 1.4 μm in cells sorted into Channel 1 (Fig. 4). In contrast, the density of the myotube networks in unsorted and sorted samples exhibited a stark difference. Specifically, unsorted control plates averaged 18.6 ± 3.3 myotubes/mm^2, whereas cells sorted into Channel 1 formed a significantly denser, more aligned network ($p = 0.004$) averaging 33.9 ± 3.7 tubes/mm^2.

Force production in 3D SMUs after microfluidic sorting

Finally, overall function of engineered SMUs was assessed by contractile force production on Day 16, following monolayer delamination and capture in 3D form. As shown in Figure 5, the peak isometric tetanic force production in unsorted control SMUs ($n = 8$) of 71 ± 8 μN was significantly increased ($p = 0.002$) approximately two-fold to 144 ± 17 μN in SMUs fabricated from cells sorted into Channel 1 of the Labyrinth microfluidic device.

Discussion

Cells separated with microfluidic sorting were analyzed to assess effects on the myogenic purity of the isolated population, along with capability for subsequent proliferation, differentiation, and function. Immediately following microfluidic sorting, two-fold enrichment of the myogenic population was observed in Channel 1 of the Labyrinth device. This enrichment was expected based on the design of the Labyrinth device for focusing smaller particles and cells, including satellite cells and myogenic progenitors, into Channel 1. In contrast, the fibroblast population was enriched in Channels 2, 3, and 4. Again, this result was intended, since the Labyrinth was designed to focus the larger fibroblasts into these channels. A minority population of fibroblasts were present in Channel 1, however, and a similar population of myogenic cells was captured in Channel 2, indicating that microfluidic sorting did not occur with maximal efficiency. It is expected that the overlap in the size distribution of satellite cells (8–13 μm[37,43]) and of

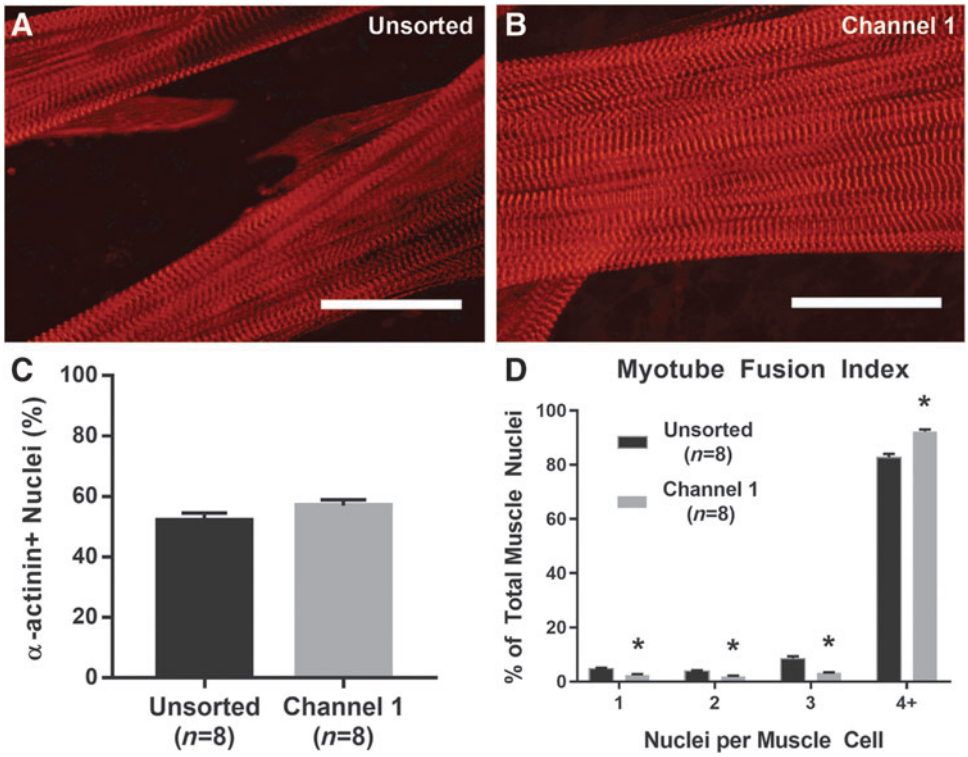

FIG. 3. Structural Maturation following Microfluidic Sorting. **(A, B)** Advanced sarcomeric structure within highly aligned myofibrils, evident from immunostaining for α-actinin, was observed on Day 11 in both unsorted controls and Channel 1 plates. Scale Bar = 50 μm. **(C)** No significant difference was recorded in the total nuclei associated with α-actinin-positive muscle cells ($p = 0.142$). **(D)** Quantification of myotube fusion index, the percentage of muscle cells with either 1, 2, 3, or 4+ nuclei, indicated greater fusion following microfluidic sorting. In particular, the percentage of fully fused myotubes with 4+ nuclei significantly increased from 82.7% ± 3.7% in unsorted controls to 92.3% ± 2.0% in Channel 1 ($p < 0.001$). * Indicates statistical difference from control.

fibroblasts (10–22 μm[53,54]) led to this reduced sorting efficiency. Alternatively, large aggregates of undigested extracellular matrix debris was observed in the microfluidic device during sorting and in outlet Channels 3 and 4 (data not shown). This debris may have impeded fluidic focusing of the different cell populations and reduced the overall sorting efficiency. Nevertheless, the majority of satellite cells and fibroblasts was consistently separated as desired by the Labyrinth device.

After microfluidic sorting, cells separated into Channel 1 were not adversely affected by the high shear forces imposed during flow through the Labyrinth device. These sorted cells exhibited similar overall proliferation to unsorted cells, in addition to improved myogenic proliferation

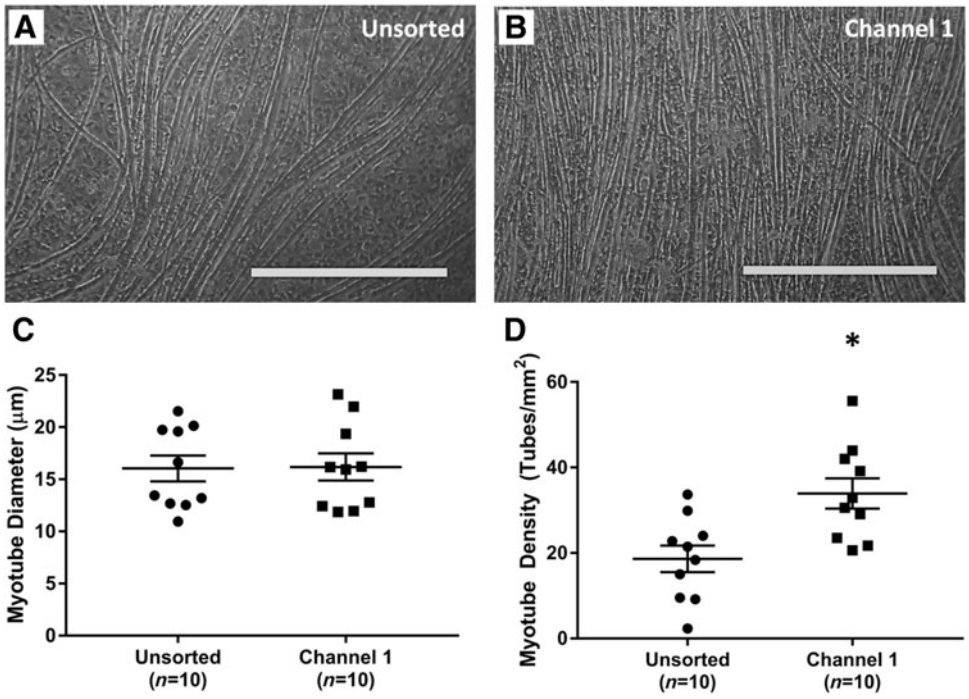

FIG. 4. Effects of Microfluidic Sorting on Myotube Growth. Shortly before delamination, light microscopy images were captured on Day 14 to assess the size and density of myotubes within the developing muscle monolayer. **(A, B)** Representative images of monolayers from unsorted cells and cell sorted into Channel 1. Scale Bar = 500 μm. **(C)** The average myotube diameter was indistinguishable between the two groups: 16.0 ± 1.3 μm in controls and 16.18 ± 1.4 μm in Channel 1 ($p = 0.938$). **(D)** Channel 1 cells, however, exhibited a significantly denser myotube network ($p = 0.004$), with 33.9 ± 3.7 tubes/mm^2 in comparison to 18.6 ± 3.3 myotubes/mm^2 in unsorted controls. * Indicates statistical difference from control.

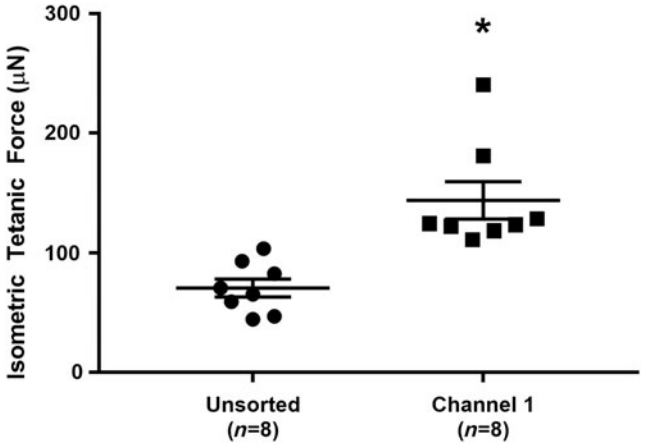

FIG. 5. SMU Functional Development with Microfluidic Sorting. Functional measurement of isometric tetanic force in 3D SMUs on Day 16 indicated a significant effect of sorting: unsorted control SMU force production of $71 \pm 8\,\mu N$ was significantly increased ($p = 0.002$) approximately two-fold to $144 \pm 17\,\mu N$ in Channel 1 SMUs. * Indicates statistical difference from control. SMU, skeletal muscle unit.

and suppression of nonmyogenic proliferation. We know that these sorted cells were more myogenically pure at seeding from our ICC analysis immediately after microfluidic separation, and observation of improved myogenic proliferation confirms this result. Improved myogenesis continued as sorted cells differentiated and fused to form a greater number of skeletal muscle myotubes. Increased myoblast fusion index was observed in cells sorted into Channel 1, resulting in a denser and highly aligned network of myotubes in the differentiation phase of SMU formation. Additionally, structural maturation of the muscle monolayers, indicated by advanced sarcomeric structure within the highly aligned myofibrils, was observed in both unsorted control and Channel 1 plates. Ultimately, these improvements in myogenic proliferation and differentiation translated to greater force production in SMUs fabricated from Channel 1 cells. In conclusion, microfluidic sorting efficiently separated satellite cells and fibroblasts while improving the capability for myogenic proliferation, differentiation, and function.

To further validate the performance of the Labyrinth device in purifying myogenic cells, it would be interesting to elucidate the specific mechanism by which the sorting process leads to improved myogenesis. This study clearly demonstrated how microfluidic sorting increased the myogenic proportion and decreased the fibrogenic proportion of the cells sorted into Channel 1. It is expected that limiting this fibroblast population and its potential to out-compete the myogenic cells for nutrients translated to the improved myogenic proliferation, differentiation, and function described above. Another possible explanation, however, is that the sorting process removed much of the tissue debris remaining from the enzymatic digestion process. Because of the design of the Labyrinth, this debris is focused into Channels 3 and 4 and removed from Channels 1 and 2. As a result, the sorted cells may not experience the same level of apoptotic signaling as unsorted cells. Future studies will investigate this possibility and seek to clarify the mechanism of action.

In conclusion, the microfluidic sorting process demonstrated in this study offers an alternative approach to purification of satellite cells enzymatically digested from a muscle biopsy. The most comparable approach, preplating to remove rapidly adhering nonmyogenic cells, can achieve greater than 80% myogenic purity.[39] The primary drawbacks to preplating, however, are the length of time required (up to 5 days) and the potential for decreased cell yields. Recently, purification of isolated satellite cells through FACS has gained popularity due to its ability to rapidly sort Pax7+ satellite cells with greater than 90% purity.[40,41] With FACS, labeling with exogenous dyes is required, and incubation with these antibodies decreases throughput. Microfluidic sorting has the potential to fill a niche distinct from these established methods. This study demonstrated a label-free sorting process requiring approximately 5 min with minimal sample preparation. The high-throughput nature of microfluidic sorting is an improvement relative to the preplating technique, and label-free purification presents an advantage over FACS and MACS, especially when separating satellite cells lacking consistent surface markers. Although the myogenic purity of cells separated with the Labyrinth devices was slightly lower than these other techniques, the benefits illustrated in this study make microfluidic sorting a promising alternative.

Acknowledgments

The authors would like to acknowledge the support of the NIH R56 grant: 2-R56-AR-054778-06-A1 and the Microfluidics in Biomedical Sciences Training Program: NIH NIBIB T32 EB005582. Additionally, the assistance of Dr. Chris Mendias in providing transgenic mice was essential to the validation of the microfluidic device.

Disclosure Statement

The authors have no competing financial interests to disclose.

References

1. Järvinen, T.A.H., Järvinen, T.L.N., Kääriäinen, M., Kalimo, H., and Järvinen, M. Muscle injuries: biology and treatment. Am J Sports Med **33,** 745, 2005.
2. Turner, N., and Badylak, S. Regeneration of skeletal muscle. Cell Tissue Res **347,** 759, 2012.
3. Huard, J., Li, Y., and Fu, F.H. Muscle injuries and repair: current trends in research. J Bone Joint Surg **84,** 822, 2002.
4. Shadrach, J.L., and Wagers, A.J. Stem cells for skeletal muscle repair. Philos Trans R Soc Lond B Biol Sci **366,** 2297, 2011.
5. Tedesco, F.S., Dellavalle, A., Diaz-Manera, J., Messina, G., and Cossu, G. Repairing skeletal muscle: regenerative potential of skeletal muscle stem cells. J Clin Invest **120,** 11, 2010.
6. Grogan, B.F., and Hsu, J.R. Volumetric muscle loss. J Am Acad Orthop Surg **19 Suppl 1,** S35, 2011.
7. Menetrey, J., Kasemkijwattana, C., Fu, F.H., Moreland, M.S., and Huard, J. Suturing versus immobilization of a muscle laceration. Am J Sports Med **27,** 222, 1999.
8. Mertens, J.P., Sugg, K.B., Lee, J.D., and Larkin, L.M. Engineering muscle constructs for the creation of func-

tional engineered musculoskeletal tissue. Regen Med **9,** 89, 2014.
9. Greene, T.L., and Beatty, M.E. Soft tissue coverage for lower-extremity trauma: current practice and techniques. J Orthop Trauma **2,** 173, 1988.
10. Lin, C., Lin, Y., Yeh, J., and Chen, C. Free functioning muscle transfer for lower extremity posttraumatic composite structure and functional defect. Plast Reconstr Surg **119,** 2118, 2007.
11. Emery, A.E. The muscular dystrophies. Lancet **359,** 687, 2002.
12. Mercuri, E., and Muntoni, F. Muscular dystrophies. Lancet **381,** 845, 2013.
13. Wicklund, M.P. The muscular dystrophies. Continuum (Minneap Minn) **19,** 1535, 2013.
14. Bushby, K. Diagnosis and management of Duchenne muscular dystrophy, part 1: diagnosis, and pharmacological and psychosocial management. Lancet Neurol **9,** 77, 2010.
15. Cossu, G., and Sampaolesi, M. New therapies for Duchenne muscular dystrophy: challenges, prospects and clinical trials. Trends Mol Med **13,** 520, 2007.
16. Deconinck, N. Pathophysiology of duchenne muscular dystrophy: current hypotheses. Pediatr Neurol **36,** 1, 2007.
17. Badylak, S.F., Taylor, D., and Uygun, K. Whole-organ tissue engineering: decellularization and recellularization of three-dimensional matrix scaffolds. Annu Rev Biomed Eng **13,** 27, 2011.
18. Beattie, A., Gilbert, T., Guyot, J., Yates, A., and Badylak, S. Chemoattraction of progenitor cells by remodeling extracellular matrix scaffolds. Tissue Eng Part A **15,** 1119, 2009.
19. Li, Q., Bai, Y., Xu, Y., and Yu, H. Autografting satellite cells to repair damaged muscle induced by repeated compression: an animal model. Foot Ankle Int **31,** 706, 2010.
20. Rando, T.A., and Blau, H.M. Primary mouse myoblast purification, characterization, and transplantation for cell-mediated gene therapy. J Cell Biol **125,** 1275, 1994.
21. Bach, A.D., Stern-Straeter, J., Beier, J.P., Bannasch, H., and Stark, G.B. Engineering of muscle tissue. Clin Plast Surg **30,** 589, 2003.
22. Corona, B.T., Machingal, M.A., Criswell, T., *et al.* Further development of a tissue engineered muscle repair construct in vitro for enhanced functional recovery following implantation in vivo in a murine model of volumetric muscle loss injury. Tissue Eng Part A **18,** 1213, 2012.
23. Juhas, M., Engelmayr, G.C., Fontanella, A.N., Palmer, G.M., and Bursac, N. Biomimetic engineered muscle with capacity for vascular integration and functional maturation in vivo. Proc Natl Acad Sci U S A **111,** 5508, 2014.
24. Larkin, L.M., Calve, S., Kostrominova, T.Y., and Arruda, E.M. Structure and functional evaluation of tendon-skeletal muscle constructs engineered in vitro. Tissue Eng **12,** 3149, 2006.
25. Lee, P.H.U., and Vandenburgh, H.H. Skeletal muscle atrophy in bioengineered skeletal muscle: a new model system. Tissue Eng Part A **19,** 2147, 2013.
26. Asakura, A., Seale, P., Girgis-Gabardo, A., and Rudnicki, M.A. Myogenic specification of side population cells in skeletal muscle. J Cell Biol **159,** 123, 2002.
27. Sherwood, R.I., Christensen, J.L., Conboy, I.M., *et al.* Isolation of adult mouse myogenic progenitors: functional heterogeneity of cells within and engrafting skeletal muscle. Cell **119,** 543, 2004.
28. Péault, B., Rudnicki, M., Torrente, Y., *et al.* Stem and progenitor cells in skeletal muscle development, maintenance, and therapy. Mol Ther Oncolytics **15,** 867, 2007.
29. Fishman, J.M., Tyraskis, A., Maghsoudlou, P., *et al.* Skeletal muscle tissue engineering: which cell to use? Tissue Eng Part B Rev **19,** 503, 2013.
30. Mauro, A. Satellite cell of skeletal muscle fibers. J Biophys Biochem Cytol **9,** 493, 1961.
31. Syverud, B.C., Lee, J.D., VanDusen, K.W., and Larkin, L.M. Isolation and purification of satellite cells for skeletal muscle tissue engineering. J Regen Med **3,** 117, 2014.
32. Allen, R.E., Temm-Grove, C.J., Sheehan, S.M., and Rice, G. Skeletal muscle satellite cell cultures. Methods Cell Biol **52,** 155, 1997.
33. Danoviz, M.E., and Yablonka-Reuveni, Z. Skeletal muscle satellite cells: background and methods for isolation and analysis in a primary culture system. Methods Mol Biol **798,** 21, 2012.
34. Bischoff, R. Enzymatic liberation of myogenic cells from adult rat muscle. Anat Rec **180,** 645, 1974.
35. Bischoff, R. Proliferation of muscle satellite cells on intact myofibers in culture. Dev Biol **115,** 129, 1986.
36. Rosenblatt, J.D., Lunt, A.I., Parry, D.J., and Partridge, T.A. Culturing satellite cells from living single muscle fiber explants. In Vitro Cell Dev Biol Anim **31,** 773, 1995.
37. Conboy, M.J., and Conboy, I.M. Preparation of adult muscle fiber-associated stem/precursor cells. Methods Mol Biol **621,** 149, 2010.
38. Richler, C., and Yaffe, D. The in vitro cultivation and differentiation capacities of myogenic cell lines. Dev Biol **23,** 1, 1970.
39. Tebbets, J., Péault, B., Crisan, M., *et al.* Isolation of a slowly adhering cell fraction containing stem cells from murine skeletal muscle by the preplate technique. Nat Protoc **3,** 1501, 2008.
40. Montarras, D., Morgan, J., Collins, C., *et al.* Direct isolation of satellite cells for skeletal muscle regeneration. Science **309,** 2064, 2005.
41. Bosnakovski, D., Xu, Z., Li, W., *et al.* Prospective isolation of skeletal muscle stem cells with a Pax7 reporter. Stem Cells **26,** 3194, 2008.
42. Pasut, A., Oleynik, P., and Rudnicki, M.A. Isolation of muscle stem cells by fluorescence activated cell sorting cytometry. Methods Mol Biol **798,** 53, 2012.
43. Chapman, M.R., Balakrishnan, K.R., Li, J., *et al.* Sorting single satellite cells from individual myofibers reveals heterogeneity in cell-surface markers and myogenic capacity. Integr Biol (Camb) **5,** 692, 2013.
44. Jankowski, R.J., Haluszczak, C., Trucco, M., and Huard, J. Flow cytometric characterization of myogenic cell populations obtained via the preplate technique: potential for rapid isolation of muscle-derived stem cells. Hum Gene Ther **12,** 619, 2001.
45. Beliakova-Bethell, N., Massanella, M., White, C., *et al.* The effect of cell subset isolation method on gene expression in leukocytes. Cytometry A **85,** 94, 2014.
46. Blanco-Bose, W.E., Yao, C., Kramer, R.H., and Blau, H.M. Purification of mouse primary myoblasts based on α7 integrin expression. Exp Cell Res **265,** 212, 2001.
47. Park, Y.G., Moon, J.H., and Kim, J. A comparative study of magnetic-activated cell sorting, cytotoxicity and preplating for the purification of human myoblasts. Yonsei Med J **47,** 179, 2006.
48. Carbonaro, A., Mohanty, S.K., Huang, H., Godley, L.A., and Sohn, L.L. Cell characterization using a protein-functionalized pore. Lab Chip **8,** 1478, 2008.
49. Segre, G., and Silberberg, A. Radial particle displacements in poiseuille flow of suspensions. Nature **189,** 209, 1961.

50. Di Carlo, D. Inertial microfluidics. Lab Chip **9,** 3038, 2009.
51. Lee, D.J., Brenner, H., Youn, J.R., and Song, Y.S. Multiplex particle focusing via hydrodynamic force in viscoelastic fluids. Sci Rep **3,** 3258, 2013.
52. Gossett, D.R., Weaver, W.M., Mach, A.J., *et al.* Label-free cell separation and sorting in microfluidic systems. Anal Bioanal Chem **397,** 3249, 2010.
53. Akhoondi, M., Oldenhof, H., Stoll, C., Sieme, H., and Wolkers, W.F. Membrane hydraulic permeability changes during cooling of mammalian cells. Biochim Biophys Acta **1808,** 642, 2011.
54. Jester, J.V., Brown, D., Pappa, A., and Vasiliou, V. Myofibroblast differentiation modulates keratocyte crystallin protein expression, concentration, and cellular light scattering. Invest Ophthalmol Vis Sci **53,** 770, 2012.
55. Lin, E., Rivera-Baez, L., Fouladdel, S., *et al.* High throughput microfluidic labyrinth for the label free isolation of CTCs for single cell gene expression profiling. Cell Syst 2017 DOI: 10.1016/j.cels.2017.08.012; [Epub ahead of print].
56. Weist, M.R., Wellington, M.S., Bermudez, J.E., *et al.* TGFβ1 enhances contractility in engineered skeletal muscle. J Tissue Eng Regen Med **7,** 562, 2013.
57. Williams, M.L., Kostrominova, T.Y., Arruda, E.M., and Larkin, L.M. Effect of implantation on engineered skeletal muscle constructs. J Tissue Eng Regen Med **7,** 434, 2013.
58. VanDusen, K.W., Syverud, B.C., Williams, M.L., Lee, J.D., and Larkin, L.M. Engineered skeletal muscle units for repair of volumetric muscle loss in the tibialis anterior muscle of a rat. Tissue Eng Part A **20,** 2920, 2014.
59. Committee for the Update of the Guide for the Care and Use of Laboratory Animals. Guide for the Care and use of Laboratory Animals: Eighth Edition. Washington, DC: National Academies Press, 2010.
60. Syverud, B.C., VanDusen, K.W., and Larkin, L.M. Effects of dexamethasone on satellite cells and tissue engineered skeletal muscle units. Tissue Eng Part A **22,** 480, 2016.
61. Costa, M. Cytoskeleton and adhesion in myogenesis. ISRN Dev Biol **2014,** 1, 2014.
62. Mills, M., Yang, N., Weinberger, R., *et al.* Differential expression of the actin-binding proteins, alpha -actinin-2 and −3, in different species: implications for the evolution of functional redundancy. Hum Mol Genet **10,** 1335, 2001.
63. van der Ven, P.F., Schaart, G., Jap, P.H., Sengers, R.C., Stadhouders, A.M., and Ramaekers, F.C. Differentiation of human skeletal muscle cells in culture: maturation as indicated by titin and desmin striation. Cell Tissue Res **270,** 189, 1992.
64. Dennis, R.G., and Kosnik II, P.E. Excitability and isometric contractile properties of mammalian skeletal muscle constructs engineered in vitro. In Vitro Cell Dev Biol Anim **36,** 327, 2000.
65. Kosnik, P.E., Faulkner, J.A., and Dennis, R.G. Functional development of engineered skeletal muscle from adult and neonatal rats. Tissue Eng **7,** 573, 2001.

Address correspondence to:
Lisa M. Larkin, PhD
Department of Molecular and Integrated Physiology
University of Michigan
109 Zina Pitcher Place, 2025 BSRB
Ann Arbor, MI 48109

E-mail: llarkin@umich.edu

Received: July 5, 2017
Accepted: September 12, 2017
Online Publication Date: November 6, 2017